CrystEngComm

PAPER

Cite this: *CrystEngComm*, 2017, **19**, 5223

Received 15th June 2017,
Accepted 31st July 2017

DOI: 10.1039/c7ce01118k

rsc.li/crystengcomm

Halogen-bonded solvates of tetrahaloethynyl cavitands†

Lotta Turunen,[a] Fangfang Pan,*[b] Ngong Kodiah Beyeh,*[cd] Mario Cetina,[ae] John F. Trant,[d] Robin H. A. Ras[c] and Kari Rissanen*[a]

The formation and structures of halogen-bonded solvates of three different tetrahaloethynyl cavitands with acetone, chloroform, acetonitrile, DMF and DMSO were prepared and investigated. The inclusion and host–guest behaviour of the resorcinarene cavitands was found to be highly dependent on the flexibility of the ethylene-bridging unit.

Halogen bonding (XB) has been receiving considerably increasing attention as it provides a complementary interaction to hydrogen bonding (HB).[1,2] XB has been proven to play crucial roles in supramolecular chemistry,[3,4] nanoscience,[5] biosystems,[6] and functional materials.[5] Its directionality and tunability make XB an important non-covalent interaction, geometrically and thermodynamically, similar to HB; however, its allowance for hydrophobicity makes it a complementary force to hydrophilic HB.[7] To exploit this interaction, many macrocyclic host molecules, functionalized with classical XB donor/acceptor pairs, have been designed.[8–13] Resorcinarenes,[14a] a subclass of the calixarene family, result from the condensation reaction of resorcinol and an aldehyde, with a π-basic cavity that has been shown to bind organic cations.[14b,c] Easily available resorcinarene derivatives have been extensively studied due to their tuneable cavity size, solubility profile, and ligand specificity.[10–13] Recently, we reported a series of pre-organized resorcinarene cavitands functionalized with four haloethynyl moieties.[13] As part of our program to construct halogen-bonded capsules, we first investigated their XB donor ability using standard XB acceptors: the oxygen in 1,4-dioxane, the sp^2 nitrogen in pyridine, and the bromide anion of tetrapropyl ammonium bromide.[13] The results provided some insight into the specific features of these resorcinarene cavitand XB receptors, not only their XB related behaviour, but also their structural features in the solid-state.

To rationally design and selectively assemble a halogen-bonded capsule, it is necessary to understand the binding preferences of these macrocyclic XB donors with different solvents. As each solvent has unique polarity, acidity, hydrophobicity and nucleophilicity properties, the halogen-bonding interactions between the XB donor and the solvent molecules have been found to be very sensitive to the nature of the solvent.[15] Studying different resorcinarene cavitand XB donors in various solvents can shed light on the efficiency of halogen bonding. This allows us to extract, from the resulting crystal structures, an understanding of the basic factors that influence the formation and properties of different solvates. The role of the solvent in halogen bonding is often unpredictable and one cannot foresee if the solvent acts as an XB acceptor or just a passive solvent. In the current contribution, we present a detailed study of the crystallization of three tetrahaloethynyl cavitands (the rigid methylene-bridged bromo- and iodoethynyl cavitands **1** and **2**, and the more flexible ethylene-bridged iodoethynyl cavitand, **3**, Fig. 1) from several different solvents.

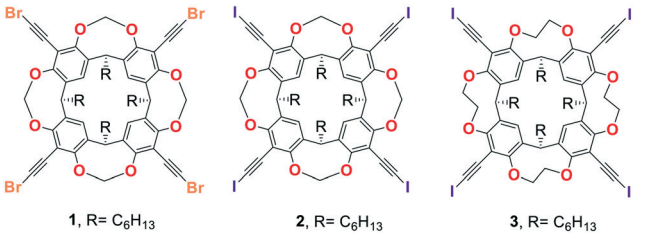

Fig. 1 The chemical structures of the tetrahaloethynyl cavitands **1**–**3**.

[a] *Department of Chemistry, University of Jyvaskyla, Nanoscience Centre, P. O. Box 35, 40014 Jyvaskyla, Finland. E-mail: kari.t.rissanen@jyu.fi; Tel: +358 50 562 3721*
[b] *Key Laboratory of Pesticide & Chemical Biology of Ministry of Education, Hubei International Scientific and Technological Cooperation Base of Pesticide and Green Synthesis, Department of Chemistry, Central China Normal University, Wuhan 430079, People's Republic of China*
[c] *School of Science, Department of Applied Physics, Aalto University, Puumiehenkuja 2, FI-02150 Espoo, Finland*
[d] *Department of Chemistry and Biochemistry, University of Windsor, N9B 3P4 Windsor, ON, Canada*
[e] *Department of Applied Chemistry, Faculty of Textile Technology, University of Zagreb, Prilaz baruna Filipovića 28a, HR-10000 Zagreb, Croatia*

† Electronic supplementary information (ESI) available. CCDC 1556027–1556033. For ESI and crystallographic data in CIF or other electronic format see DOI: 10.1039/c7ce01118k

Crystallization of the three tetrahaloethynyl cavitands from acetone, chloroform, acetonitrile, DMF, and a $CHCl_3$–DMSO mixture was performed. A total of seven crystalline solvates were obtained from these experiments: **1**·acetone, **1**·$CHCl_3$, **2**·MeCN, **2**·DMF, **3**·DMF, **3**·DMSO, and **3**·acetone.

Two solvates, **1**·$CHCl_3$ and **1**·acetone, from bromoethynyl-functionalized resorcinarene cavitand **1**, and the MeCN solvate **2**·MeCN from iodoethynyl-substituted cavitand **2** are surprisingly isostructural, crystallizing in the monoclinic space group $P2_1/n$ (Fig. 2) with very similar unit cell parameters. In each case, the asymmetric unit contains one tetrahaloethynyl cavitand and one solvent molecule enclosed in the concave space between the lower rim hexyl tails. The cavitand–solvent unit appears in the crystal lattice as a self-included dimer (see below). Only very weak C–H···O/N/Cl hydrogen bonds were observed between the α-carbon hydrogen of the lower rim hexyl chains and the solvent. The flexibility of the hexyl chains induces a slight disorder of the enclosed solvent. The self-inclusion behaviour of these tetrahaloethynyl cavitands is similar to that of the tetraiodoethynyl cavitand structures previously reported by us.[14]

In the crystal structure of **2**·MeCN, the steric fit of the iodoethynyl group into the cavity of the adjacent cavitand is reinforced by several weak C–H···C≡C triple bond interactions that drive the formation of the self-included dimer. This can be visualized using a Hirshfeld surface analysis[16] of the interactions between the cavitand bridging methylene group hydrogen and the triple bond of the self-included dimer pair, as shown by green broken lines in Fig. 3a. The large white surface at the molecular interface between the dimers indicates the existence of significant van der Waals interactions, explaining the close packing of adjacent dimers. In **1**·$CHCl_3$, **1**·acetone, and **2**·MeCN, along the self-inclusion axis (the crystallographic *c*-axis), weak intermolecular Br···O XBs link adjacent dimers into a one dimensional (1D) chain (Fig. 4 and S2†).

Two additional symmetric Br···O halogen bonds (Fig. 4 and S1A†) bridge the adjacent self-included dimers and have short interaction ratios ($R_{XB} = d_{XB}/(X_{vdw} + B_{vdw})$),[17] R_{XB} = 0.97 in **1**·acetone, 0.97 in **1**·$CHCl_3$ and 0.95 in **2**·MeCN. Along the crystallographic *a*-axis, the arrangement of the molecules indicates a weak Br···π contact, with a Br···C (closest phenyl carbon atom) distance of 3.4301(2) Å for **1**·acetone (Br1···C25_x − 1, y, z), 3.59422(6) Å for **1**·$CHCl_3$ (Br3···C2_x − 1, y, z), and 3.39356(5) Å for **2**·MeCN (I2···C33_1 + x, y, z). These halogen bonding interactions are visible from the Hirshfeld surface plots. Although weak, these XBs are clearly

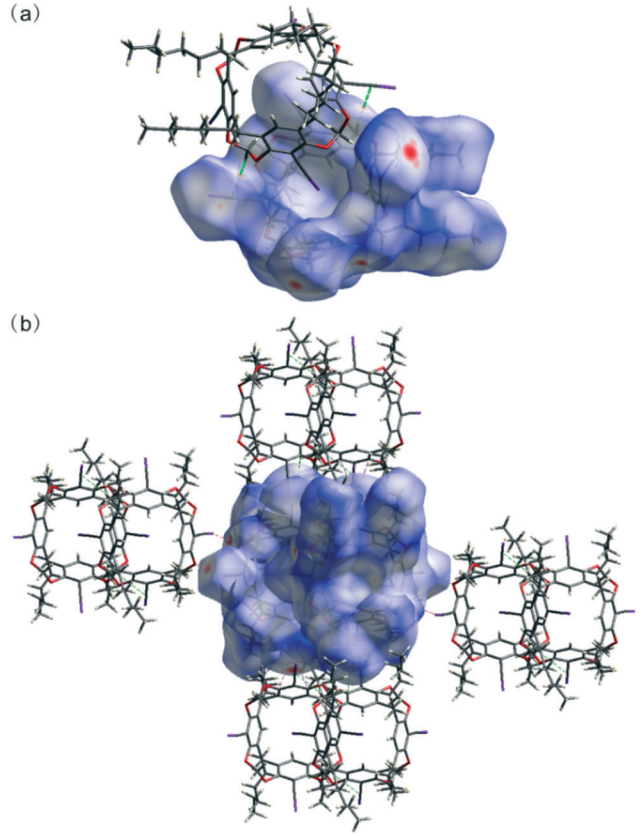

Fig. 3 The X-ray structure of **2**·MeCN: (a) *d*-norm type Hirshfeld surface analysis showing the non-covalent interactions between the self-included dimers, one unit of which is represented by the surface, and (b) a zoomed-out view showing the molecular packing between dimeric units. Color code: grey, C; white, H; red, O; purple, I.

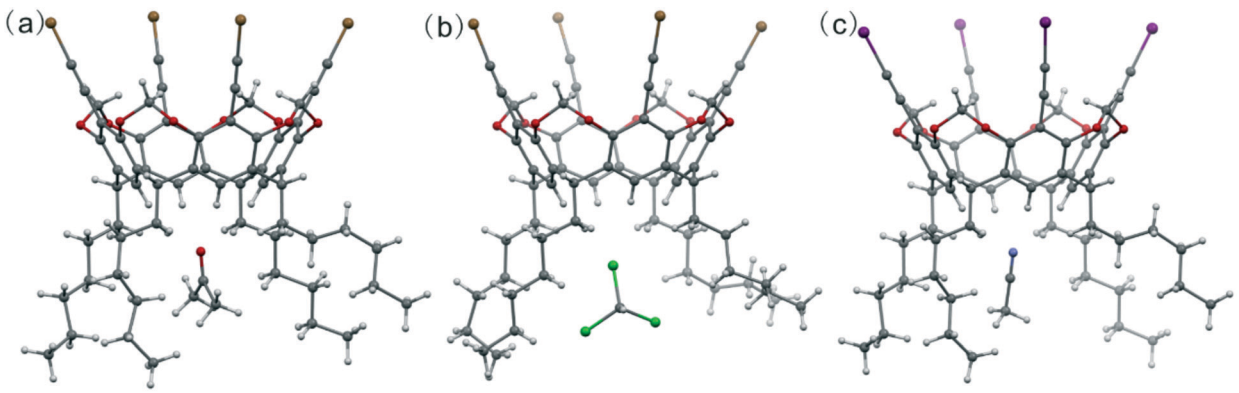

Fig. 2 Isostructural solvates (a) **1**·acetone, (b) **1**·$CHCl_3$, and (c) **2**·MeCN in ball-and-stick models. Color code: grey, C; white, H; red, O; blue, N; green, Cl; brown, Br; purple, I.

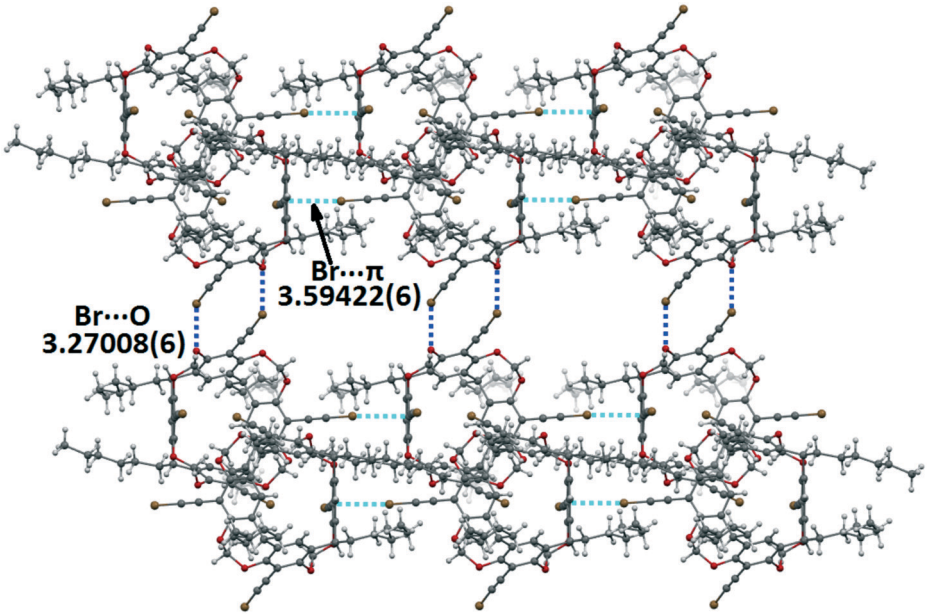

Fig. 4 A visualization of the self-assembly of **1**·$CHCl_3$ into 2-dimensional sheets. The secondary bonding between adjacent resorcinarene cavitands along the crystallographic *b*-(cyan for Br···π) and *c*-axes (blue for Br···O) is organized through intermolecular halogen bonds. The distance for the Br···π interaction was calculated using the closest Br and carbon atoms, Br···C2. Color code: grey, C; white, H; red, O; blue, N; brown, Br. A similar packing is observed with **1**·acetone and **2**·MeCN.

essential for the crystal packing. The Hirshfeld surface analysis also allows for a statistical evaluation of the packing interactions. For example, in the case of **2**·MeCN, the H···H contacts comprise almost 38.8% of all non-covalent interactions, while the C···H contacts provide an additional 17.1% of all intermolecular interactions (Fig. S3†). We were not successful in getting crystals of DMF and DMSO solvates using bromoethynyl **1**, but managed to obtain them using iodoethylene cavitands **2** and **3**.

The O-atom in the DMF molecule can be a good XB acceptor, particularly when iodine is the XB donor. Suitable crystals of tetraiodoethynyl cavitand **2** were grown in chloroform containing a few drops of DMF to provide the **2**·DMF solvate. In this structure, the asymmetric unit contains only half of the cavitand molecule, with half an arbitrarily assigned DMF molecule in between the lower rim of the cavitand, a quarter of a DMF molecule interacting with I1 *via* XB, and another disordered DMF molecule interacting with I2 *via* XB. Three of the four **2**·DMF iodoethynyl groups participate in XBs with the oxygen atoms of three different DMF molecules (Fig. S1d†), while the fourth iodoethynyl group is embedded into the cavity of a second cavitand to form a self-included dimer.

These moderately strong XBs lead to smaller R_{XB} values (0.8 in average) than those observed for bromoethynyl **1** and are in line with those reported previously for the **2**·dioxane structure.[14] Unlike the **1**·solvates (which used XB interactions), the structure extends along the crystallographic *c*-axis through π···π interactions between the phenyl groups from two cavitands (Fig. 5a). It is worth mentioning that only one side of the cavitand is involved in the π···π interactions due to the lattice symmetry.

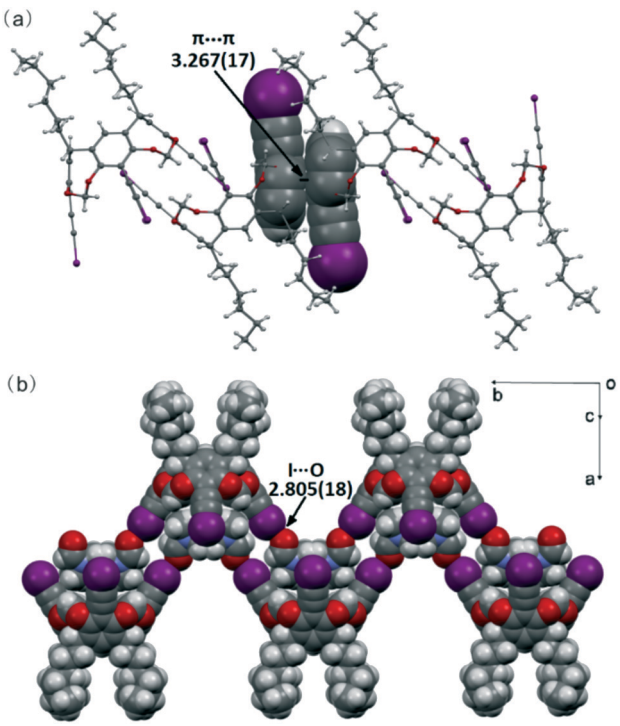

Fig. 5 Halogen-bonded **2**·DMF: (a) π···π interaction between adjacent cavitands that induces dimer formation, the π···π distance was calculated using the closest carbon atoms in the phenyl rings, C3···C3_1 − *x*, *y*, −*z*; (b) an extension of this self-assembly pattern through the (−1 0 1) plane. The neighbouring π···π interacting iodoethynyl benzene rings in (a) and the whole structure in (b) are in CPK mode. Color code: grey, C; white, H; red, O; blue, N; purple, I.

In addition to the halogen-bonded DMF molecule in the 2·DMF solvate, a symmetry-induced disordered second DMF molecule occupies the cavity of the resorcinarene cavitand. Likewise, a third DMF molecule is located between the lower rims of the cavitand instead of the regular solvent molecules seen in the cavitand 1 structures. The disordered cavity-based DMF molecule with its oxygen atom pointing upwards forms an XB with the iodine of a vertically adjacent cavitand, extending the interactions into 1D-chains along the (−1 0 1) plane (Fig. 5b).

Unlike the rigid methylene cavitands 1 and 2, the ethylene bridges increase the internal volume of the cavity and the flexibility of cavitand 3. Thus, the more open cavity has C_{2v} symmetry instead of the pseudo-C_{4v} symmetry of 1 and 2 (Fig. 6). In our previous work,[14] we reported that the more flexible cavitand 3 has a much weaker tendency to form self-included dimers. This implies that all four iodine atoms will be available as XB donors. In the present work, only one solvate of cavitand 3 demonstrates pure self-inclusion behaviour, *viz.* 3·DMF. However, in 3·DMF the self-inclusion manifests differently from those of 1 and 2, as the iodoethynyl group of the first cavitand 3 fills the cavity of the second cavitand 3. However, the iodoethynyl group of the second cavitand 3 does not fill the cavity of the first one (Fig. 6a). This off-axis self-inclusion arrangement breaks the centre of symmetry, leaving seven XB donor sites free. Interestingly, only five out of these seven iodine atoms are involved in XBs with the oxygen atoms of DMF, leaving two iodine atoms free for additional interactions. Besides, the dimer includes two non-XB DMF molecules, each entrapped between the lower hexyl groups of each cavitand 3. Among the five halogen-bonded DMF molecules, one is trapped in the cavity of the neighboring off-axis self-inclusion dimer, whose XB-DMF also punctures into the cavity of the first dimer (Fig. 6b). In this sense, the assembly can be regarded as a 4 : 8 XB complex (4 cavitands with eight halogen-bonded DMF molecules). The π···π interactions between the phenyl faces of adjacent cavitands are also observed in the lattice of 3·DMF. The π···π interactions extend the molecular arrangement along the crystallographic *c*-axis (Fig. 6c).

The structure of 3·DMSO (Fig. 7) is quite different from that of 3·DMF. Instead of a direct self-inclusion dimer as in other cases, one DMSO molecule is included into the cavity of 3. This cavity residing DMSO molecule is halogen-bonded to one iodine atom of the adjacent cavitand resulting in a 2 : 4 XB dimeric assembly, if considering the other halogen-bonded DMSO molecule for each cavitand 3 of the dimer (Fig. 7a). Of the remaining two iodine atoms of the cavitand, one is halogen-bonded with the π-electrons of the ethynyl group of the adjacent cavitand, while the second has no interactions with anything but only sits in the void between the cavitands. The I···π interactions extend the structure into 1-D threads along the crystallographic *b*-axis (Fig. 7c). There is also a face-to-face π···π interaction between the phenyl groups of two adjacent cavitands (Fig. 7b).

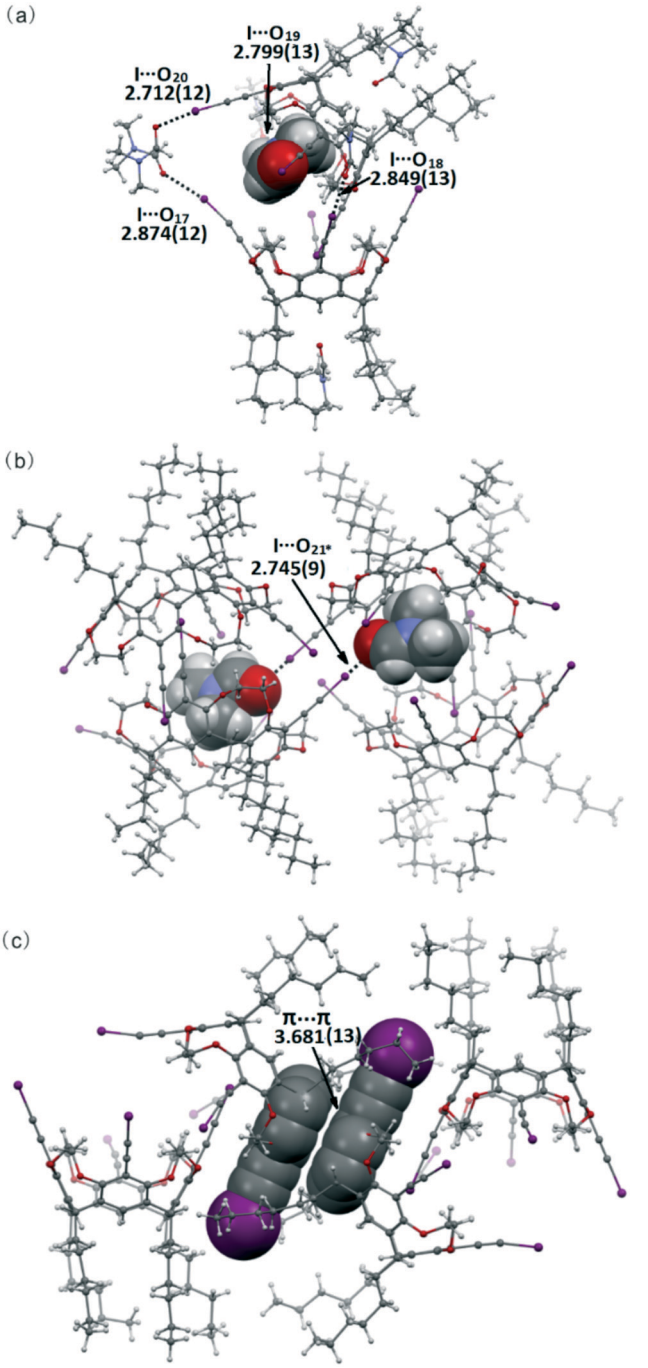

Fig. 6 Projections of 3·DMF to show: (a) the off-axis self-inclusion dimer; (b) the I···O XB connection between the neighbouring dimers with the inclusion of DMF molecules in CPK mode, and (c) the π···π interactions (3.681(13) Å) between the self-inclusion dimers with the iodoethynyl benzene groups in contact with each other in CPK mode. The * represents the symmetry of 1 − *x*, 1 − *y*, 1 − *z*. The π···π distance was calculated using the closest carbon atoms (C36···C39_1 − *x*, 1 − *y*, *x* − *z*). Color code: grey, C; white, H; red, O; blue, N; purple, I.

The inclusion behaviour of 3 in 3·DMSO also emerges in the 3·acetone structure as one acetone molecule is located in the cavity of cavitand 3 (Fig. 8a). The polarized iodine in the iodoethynyl unit of 3 readily forms a halogen bond with the

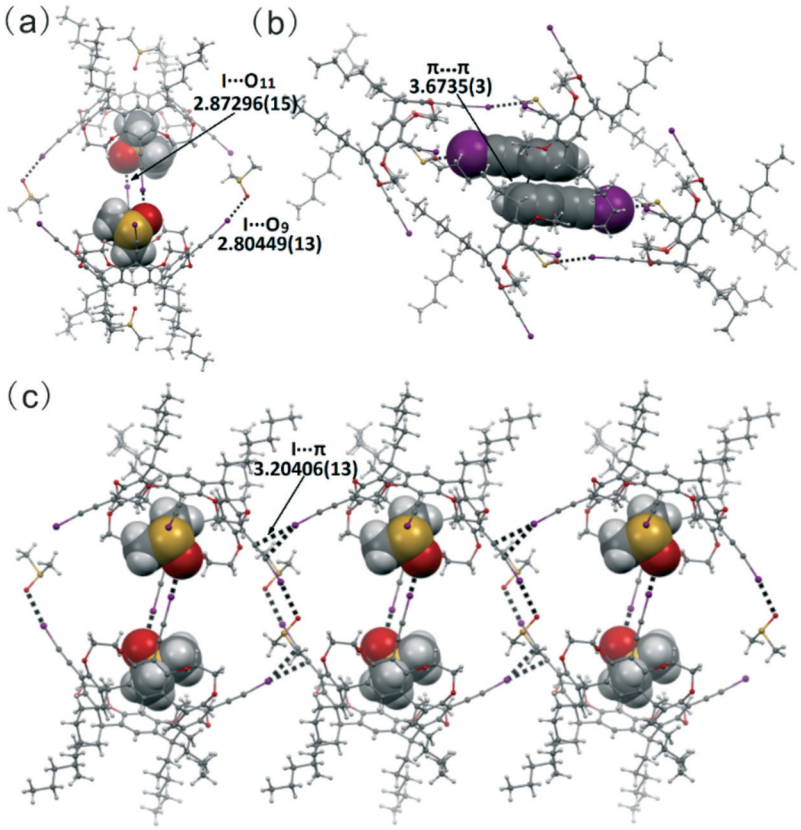

Fig. 7 (a) Solvent involved in the self-inclusion dimer in the structure of **3**·DMSO; (b) the π···π interaction and (c) the I···π XBs between the dimers. The π···π distance given in (b) was calculated using the closest carbon atoms (C1···C4_2 − *x*, 1 − *y*, 2 − *z*); the I···π distance in (c) was calculated using I2···C58_*x*, 1 + *y*, *z*. Color code: grey, C; white, H; red, O; brown, Br; purple, I.

acetone oxygen. Two of the four iodo groups participate in the I···O XBs, assembling the solvate into a 2 : 4 XB complex (2 cavitands with four halogen-bonded acetone molecules). In addition, the third iodide is involved in an I···$O_{cavitand}$ XB (Fig. 8c), and π···π contacts stabilize the facing phenyl groups from two adjacent cavitands (Fig. 8b).

The seven solvates studied in this work include two for cavitand **1**, two for cavitand **2** and three for cavitand **3**. **1**·acetone, **1**·$CHCl_3$, and **2**·MeCN are isostructural. We attribute the reason for this phenomenon to the weak ability of the cavitand and the solvent to form a halogen bond, as compared to the stronger interactions both within, and between adjacent, cavitands. Although acetonitrile is often regarded as a good XB acceptor, a CSD survey reveals that only a few weak XB solvates from acetonitrile were reported (13 hits for an I···N distance from 2.895 to 3.482 Å with an average of 3.261 Å; 20 hits for a Br···N distance from 2.837 to 2.366 Å with an average of 3.228 Å).[18] The solvent molecules in these structures were trapped between the hexyl groups in the lower rim of the cavitands *via* CH···O/N/Cl interactions. Due to lack of XBs between the cavitand and solvents, the interactions between the cavitands are responsible for the molecular packing in the crystal lattice. The introduction of DMF to cavitand **2** breaks the packing pattern, due to XB formation between **2** and DMF, although the self-inclusion behaviour was preserved. These XB forces also create relatively larger lattice pores, which in turn result in the disordered distribution of the DMF molecules. XB interactions between cavitand **3** and the solvent molecule exist in **3**·DMF, **3**·DMSO and **3**·acetone. Supramolecular synthons such as I···O XB, π···π and I···$\pi_{ethynylbenzene}$ forces are all similar in the solvates (no I···π in **3**·DMF). They afford completely different assemblies and packings. Taking into account the different modes of solvent-assisted inclusion dimers and the halogen-bonded solvent molecules, the three solvates form 4 : 10, 2 : 4 and 2 : 4 assemblies for **3**·DMF, **3**·DMSO and **3**·acetone, respectively (Fig. S5†). Besides, each cavitand has one solvent molecule trapped in its lower hexyl groups. Other non-XB solvents as void-filling molecules are also found in the lattices of the solvates. The differences in halogen-bonded assembly and in lattice-filling solvent cause the solvates to demonstrate a distinct packing, which in principle is not predictable.

To better understand the supramolecular synthons and structural features of the solvates, the electrostatic potentials were calculated using Spartan'14 software[19] with the DFT-B3LYP method at the 6-311+G** level for the cavitands and solvents, and the 6-311G* level for the solvates in a vacuum. The ESP maps show similar features for the three cavitands. An electropositive area on the top of the ethynyl-halo groups was observed which indicates the XB donor potential of the cavitands. Meanwhile, the electron rich regions were found

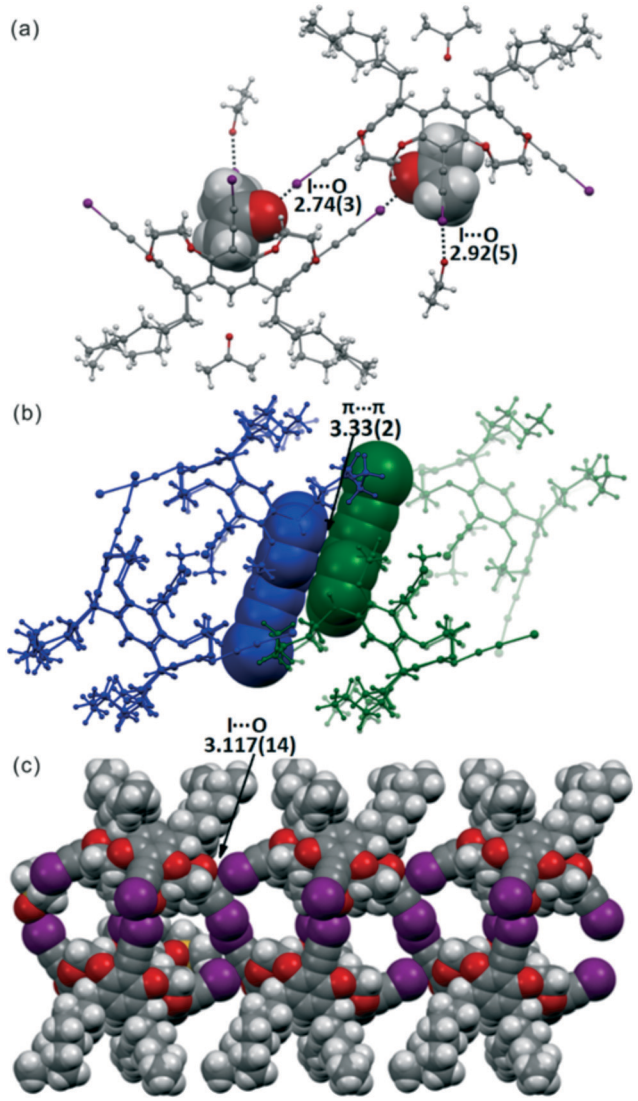

Fig. 8 Solvent assisted self-inclusion dimer in the structure of **3**·acetone (a); the π···π interactions (3.33 Å) between the self-inclusion dimers, highlighted in blue and green, respectively (b); and the I···$O_{cavitand}$ XBs extending the structure to be 1D (c). The π···π distance in (b) was calculated using the closest carbon atoms (C18···C20_1 − *x*, −*y*, 2 − *z*). The iodoethynyl benzene groups in contact with each other in (b) and the whole structure in (c) are shown in CPK mode. Colour code: grey, C; white, H; red, O; purple, I.

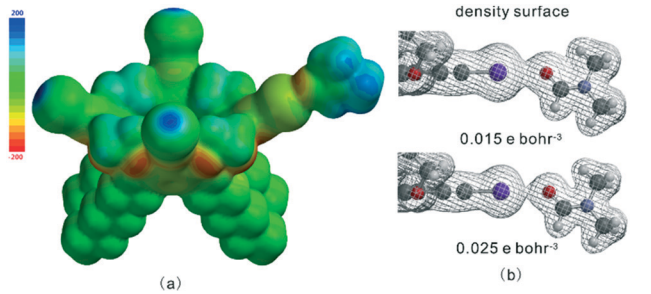

Fig. 9 The ESP mapped on the isosurface of 0.002 e $bohr^{-3}$ (a) and the electron density surfaces (b) in **3**·DMF.

in the middle belt of the cavitands, mainly on the oxygen atoms and the triple bonds. The methylene groups in **1** and **2**, as well as the ethylene group in **3**, show some electron depletion features. They could well account for the self-inclusion phenomenon (held by C–H···triple bond interaction) in the structures of **1** and **2**. Ethylene groups in **3** modify the orientation of the CH bonds that avoid the formation of self-inclusion dimers. The ESP maps for the solvent molecules show that the oxygen atoms in acetone, acetonitrile, DMF and DMSO are dramatically negatively charged. They have the ability to act as XB acceptors interacting with the ethynyl halo groups of the cavitands. The methyl groups in acetone, acetonitrile, DMF, and DMSO, and the CH in chloroform are clearly positively charged. They readily interact with the negatively charged groups in the cavitand together with other preferable secondary interactions, thus efficiently acting as lattice-filling species for the solvates. However, acetone and acetonitrile could easily escape from the crystal lattice during the crystallization due to their volatility.

The geometry optimization of the solvates was conducted at the Hartree–Fock 3–21 level starting from the geometry in the X-ray crystal structures. The resulting I···O bond distances in **3**·DMF, **3**·DMSO and **3**·acetone were 2.704, 2.633, and 2.817 Å, respectively, in line with those in the corresponding crystal structures. The ESP map on a 0.002 e $bohr^{-3}$ density surface shows connectivity for the XB adduct. The iodoethynyl group bonded with the solvent displays a more negative electrostatic potential than the others. Moreover, bonds with maximum electron density values over 0.1 e $Å^{-3}$ (≈0.015 e $bohr^{-3}$) are generally considered covalent.[20] In the current cases, the electron density surface at 0.015 e $bohr^{-3}$ (Fig. 9b and S8†) demonstrates a significant overlap between the iodine and oxygen atoms, implying the remarkable covalent component and charge transfer from the solvents to the cavitands.

Conclusions

In conclusion, seven solvates from three tetrahaloethynyl cavitands were successfully crystallized, and their crystal structures were analysed. One small (up to five non-H atoms) solvent molecule can comfortably be accommodated in the small space between the lower-rim hexyl chains of the cavitand. Unlike methylene cavitands **1** and **2**, all three structures with flexible cavitand **3** show solvent inclusion within the resorcinarene cavity. All solvates demonstrate some common features such as π···π interactions between the phenyl groups of two adjacent cavitands in the crystal lattice. The oxygen and the π system of the cavitands compete with the solvents as potential XB acceptor sites for XB interactions during the crystallization process. Quite surprisingly, acetonitrile, which should be a good XB acceptor, does not participate in any XB formation with either bromo-cavitand **1** or iodo-cavitand **2**. However, in all cases, the haloethynyl groups act as XB donors with the oxygen atoms or the π system of the cavitand. When interacting with the guest or

solvent molecules with stronger XB acceptor ability, such as DMF and DMSO, iodo-cavitand **3** shows prominent I···O halogen bonds. Our results show that the subtle interplay between the XB donor cavitands themselves and with solvent molecules as XB acceptor molecules emerges through complex and in many cases unpredictable intermolecular interactions where the fine balance between halogen and hydrogen bonding drives the crystallization process.

Acknowledgements

The authors gratefully acknowledge financial support from the Academy of Finland (KR: grant no. 265328, 263256 and 292746; RHAR: grant no. 272579), the University of Jyvaskyla, Aalto University, Finland, and the University of Windsor, Canada. This work was supported by the Program of Introducing Talents of Discipline to Universities of China (111 program, B17019) and the Academy of Finland through its Centres of Excellence Programme (HYBER 2014–2019). Dr. Kari Raatikainen is thanked for data collections for structure **1**·$CHCl_3$.

Notes and references

1 A. Mukherjee, S. Tothadi and G. R. Desiraju, *Acc. Chem. Res.*, 2014, **47**, 2514–2524.
2 G. R. Desiraju, P. S. Ho, L. Kloo, A. C. Legon, R. Marquardt, P. Metrangolo, P. Politzer, G. Resnati and K. Rissanen, *Pure Appl. Chem.*, 2013, **85**, 1711–1713.
3 P. Metrangolo, F. Meyer, T. Pilati, G. Resnati and G. Terraneo, *Angew. Chem., Int. Ed.*, 2008, **47**, 6114–6127.
4 L. C. Gilday, S. W. Robinson, T. A. Barendt, M. J. Langton, B. R. Mullaney and P. D. Beer, *Chem. Rev.*, 2015, **115**, 7118–7195.
5 (*a*) T. Shirman, T. Arad and M. E. van der Boom, *Angew. Chem., Int. Ed.*, 2010, **49**, 926–929; (*b*) A. Priimagi, G. Cavallo, P. Metrangolo and G. Resnati, *Acc. Chem. Res.*, 2013, **46**, 2686–2695.
6 M. R. Scholfield, C. M. Vander Zanden, M. Carter and P. S. Ho, *Protein Sci.*, 2013, **22**, 139–152.
7 G. Cavallo, P. Metrangolo, R. Milani, T. Pilati, A. Priimagi, G. Resnati and G. Terraneo, *Chem. Rev.*, 2016, **116**, 2478–2601.
8 H. S. El-Sheshtawy, B. S. Bassil, K. I. Assaf, U. Kortz and W. M. Nau, *J. Am. Chem. Soc.*, 2012, **134**, 19935–19941.
9 F. Zapata, A. Caballero, N. G. White, T. D. W. Claridge, P. J. Costa, V. Felix and P. D. Beer, *J. Am. Chem. Soc.*, 2012, **134**, 11533–11541.
10 O. Dumele, N. Trapp and F. Diederich, *Angew. Chem., Int. Ed.*, 2015, **54**, 12339–12344.
11 (*a*) N. K. Beyeh, F. Pan and K. Rissanen, *Angew. Chem., Int. Ed.*, 2015, **54**, 7303–7307; (*b*) L. Turunen, U. Warzok, R. Puttreddy, N. K. Beyeh, C. A. Schalley and K. Rissanen, *Angew. Chem., Int. Ed.*, 2016, **55**, 14033–14036.
12 (*a*) F. Pan, N. K. Beyeh and K. Rissanen, *J. Am. Chem. Soc.*, 2015, **137**, 10406–10413; (*b*) N. K. Beyeh, A. Valkonen, S. Bhowmik, F. Pan and K. Rissanen, *Org. Chem. Front.*, 2015, **2**, 340–345.
13 L. Turunen, N. K. Beyeh, F. Pan, A. Valkonen and K. Rissanen, *Chem. Commun.*, 2014, **50**, 15920–15923.
14 (*a*) P. Timmerman, W. Verboom and D. N. Reinhoudt, *Tetrahedron*, 1996, **52**, 2663–2704; (*b*) K. Rissanen, *Angew. Chem., Int. Ed.*, 2005, **44**, 3652–3654.
15 M. G. Sarwar, B. Dragisic, L. J. Salsberg, C. Gouliaras and M. S. Taylor, *J. Am. Chem. Soc.*, 2010, **132**, 1646–1653.
16 M. A. Spackman and D. Jayatilaka, *CrystEngComm*, 2009, **11**, 19–32.
17 (*a*) P. M. Lommerse, A. J. Stone, R. Taylor and F. H. Allen, *J. Am. Chem. Soc.*, 1996, **118**, 3108–3116; (*b*) L. Brammer, E. A. Bruton and P. Sherwood, *Cryst. Growth Des.*, 2001, **1**, 277–290; (*c*) F. Zordan, L. Brammer and P. Sherwood, *J. Am. Chem. Soc.*, 2005, **127**, 5979–5989.
18 C. R. Groom and F. H. Allen, *Angew. Chem., Int. Ed.*, 2014, **53**, 662–671. Note, the search was done with CCD Conquest version 5.36, May 2016; only structures featuring "I/Br···N≡C–Me" species were included. The species were constrained with I/Br···N distances shorter than the van der Waals' sum and the number of bonded atoms for I/Br set to 1.
19 *SPARTAN '14*, Wavefunction Inc., Irvine, CA, 2014.
20 W. J. Hehre, *A Guide to Molecular Mechanics and Quantum Chemical Calculations*, Wavefunction, Irvine, CA, 2003.